Rotor Power Savings with Active Camber Actuation Varying Baseline Rotor Properties and Operating Conditions

Dominik Komp*
Graduate Research Assistant

Manfred Hajek*
Professor and Department Head

Jürgen Rauleder[†]
Assistant Professor

Abstract

A variation of helicopter main rotor properties was investigated with regard to their effects on active camber induced power savings using a comprehensive analysis model including elastic blade modeling and free vortex wake analysis. A Bo 105 main rotor was used as the baseline rotor in this work. This study was aimed at analyzing the transferability of results on active camber induced power savings to other rotor systems, while also identifying design targets for a rotor designated to be operated with an active camber system. A range of advance ratios from 0 to 0.35 was investigated. Active camber actuation on the modified baseline rotors was examined with regard to the absolute power variation compared to the original baseline rotor, and the relative power variation compared to the modified baseline rotor. The rotor blade torsional stiffness did not prove to be an important design parameter to optimize rotor power at high-speed flight using active camber. Only the relative rotor power savings from active camber notably depended on the blade torsional stiffness. The built-in twist of the baseline Bo 105 rotor was identified to be below the optimum. This lack of efficiency was compensated by active camber. Therefore, active camber yielded a reduced capability to improve rotor power for higher geometric built-in blade twist, especially for low advance ratios. Increased efficiency of the baseline rotor, however, did not necessarily reduce the efficiency gain from active camber. This was shown in case of varying the number of rotor blades and the blade taper ratio, where greater baseline rotor efficiency still resulted in an increase of relative power savings from active camber. A reduction in rotational speed resulted in significant rotor total power savings, but had a negative effect on the power savings from active camber. However, active camber was able to ameliorate detrimental effects from a reduced rotor rotational speed on thrust and stall margins.

Notation

α	blade section angle of attack, deg
α_s	rotor shaft tilt (negative forward), deg
δ	active-camber deflection (positive downwards), deg
$\delta_{n\mathrm{P}}$	active-camber deflection amplitude of n-th harmonic component, deg
μ	advance ratio, $v/\Omega R$
Ω	angular velocity of rotor blade, rad/s
$\phi_{n\mathrm{P}}$	phase of nP active actuation input, deg
ψ	rotor azimuth (counter-clockwise), deg
ρ	density of air, $\mathrm{kg/m^3}$
σ	rotor solidity, $N_b c/\pi R$
θ_{etw}	elastic blade twist (same sign convention as θ_{tw}), deg
θ_{tw}	linear blade built-in twist (from hub to tip, tip pitch minus root pitch), deg
ϑ	spanwise variation of camber deflection, %
c	blade chord, m
C_l	2-D airfoil lift coefficient
C_T	rotor thrust coefficient (shaft axis), $T/\pi\rho R^2(\Omega R)^2$
GJ	blade torsional stiffness, $\mathrm{Nm^2}$
L	rotor lift (wind axis), N
M	Mach number
M_x	hub roll moment (shaft axis, right wing up positive), Nm
n	active control input harmonic (1/rev)
N_b	number of rotor blades
$P_{\mathrm{b,mod}}$	rotor power of the modified baseline rotor, kW
P_{b}	rotor power of the original baseline rotor, kW
R	rotor disk radius, m
r_1	radial position of inboard edge of the active-camber section, m
r_2	radial position of outboard edge of the active-camber section, m
T	rotor thrust (shaft axis), N
t	taper ratio, $c_{\mathrm{tip}}/c_{\mathrm{root}}$
v	forward flight velocity, m/s
X	rotor drag (wind axis, negative for propulsive force), N
RPM	rotor revolutions per minute

* Institute of Helicopter Technology, Technical University of Munich, Munich, Germany
[†] Georgia Institute of Technology, Atlanta, GA, USA
Presented at 47th European Rotorcraft Forum, United Kingdom, 7-9th September, 2021.

Introduction

Active rotor control mechanisms have been investigated to improve the rotor aerodynamic efficiency compared to a rotor solely based on primary control through a swashplate mechanism. This comprises mechanisms like individual blade control (IBC) or active twist control (Refs. 1–3). These approaches, however, do not influence the blade sectional aerodynamics characteristics over one rotor revolution, such as done by systems like trailing-edge (TE) flaps ore active-camber control. The effectiveness of higher-harmonic TE flap control in fast forward flight was confirmed in previous publications (Refs. 3–6).

To avoid any discontinuity on the blade surface, continuous airfoil morphing with active-camber systems has been proposed to improve rotor efficiency (Ref. 7) compared to TE flaps. This approach was found to be effective in terms of rotor power savings (Ref. 8). Also, a spanwise variation of actuation input is possible with such a system due to the necessity of using a flexible blade skin. This resulted in additional rotor power benefits, particularly in low-speed flight (Ref. 9).

This work uses an active-camber system referred to as the Fish Bone Active Camber (FishBAC); see Ref. 7. It is capable of dynamically morphing the rotor blade airfoil over one rotor revolution, which is in particular interesting for fast forward flight, but also to quasi-statically apply camber deflection as a configuration change for various flight speeds. Based on the Bo 105 isolated rotor, active camber resulted in maximum performance improvements of up to 7% over the baseline rotor power at low and high-speed flight (Ref. 9).

The mechanism of improving rotor power with active camber depends on complex aeroelastic interactions with significant influence on the elastic blade deformation and adjustments of primary control inputs. In continuation of this previous work, the objective of this current work was to investigate the influence of relevant baseline rotor properties on these complex dynamics initiated by active camber. From this, possible design targets may be identified for a rotor designated to be used in combination with an active-camber system. Furthermore, previous active versus passive rotor results obtained for the Bo 105 rotor were evaluated with regard to their transferability to other rotor systems. This comprises results with regard to efficiency gains, but also concerning the necessary actuation input characteristics to improve the understanding of employing active camber rotors.

Modeling Approach

The rotorcraft comprehensive aeromechanics analysis tool CAMRAD II was used for the current investigation. The rotor used as the baseline was a full-scale Bo 105 hingeless rotor.

Implementation of the Active Rotor Concepts

Figure 1 illustrates the parameters used to define the active-camber actuation on the rotor blade. Figure 1a specifies the deflection angle δ as the metric for measuring camber deflection. The baseline (static) airfoil was a NACA23012 and only the aft 25% of the chord were actively morphed for structural feasibility of the morphing mechanism. The chord line of the baseline airfoil shown as the dashed line in Fig. 1a was used as the reference to measure the angle of attack irrespective of the degree of camber deflection. This means that all airfoil shapes shown in Fig. 1a are at the same angle of attack. In Fig. 1b, variables defining the camber deflection during the actuation cycle (see Eq. 1) are explained. Therein, the positions marked with (ii) and (iv) represent the upper and lower limit of actuation. In case of isolated harmonic actuation, δ_{hpp} corresponds to δ_{nP}. Figure 1c illustrates the parameters r_1 and r_2 that define the blade section where the active-camber mechanism was integrated.

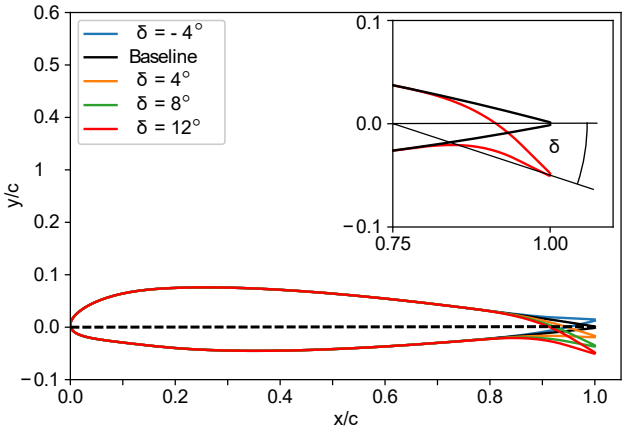

(a) Active-camber airfoils and δ definition.

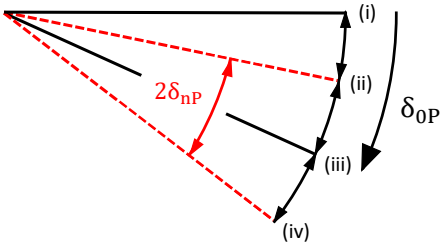

(b) Active-camber deflection with isolated harmonic input, (i) baseline, (ii) minimum deflection, (iii) mean deflection, (iv) maximum deflection.

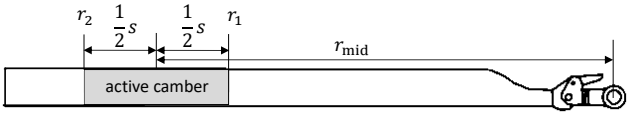

(c) Active-camber geometric parameters.

Fig. 1. Parametrization of the active-camber concept.

$$\delta = \delta_{0\mathrm{P}} + \sum_{n=1}^{2} \delta_{\mathrm{nP}} \cdot \cos(n\psi - \phi_{\mathrm{nP}}) \qquad (1)$$

Spanwise variation of camber deflection was measured with ϑ. It was defined such that the actuation cycle at the mid radial station of the active-camber section remained unaffected

compared to the original actuation input. At the inboard edge of the active-camber section, r_1, the actuation cycle changed to

$$\delta_1 = \delta \cdot (100\% + \vartheta) \tag{2}$$

and at the outboard edge, r_2, it was modified to

$$\delta_2 = \delta \cdot (100\% - \vartheta). \tag{3}$$

Structural Model

A structural model of the full-scale Bo 105 rotor was developed including a swashplate control mechanism. The radial distribution of structural properties of the blade were provided by DLR and were defined at 41 radial stations. The elastic blade motion was calculated using Euler−Bernoulli beam theory. Each blade was modeled using five beam segments along the blade span, with six rigid and seven elastic degrees of freedom per element. A comparison of the modal analysis of the CAMRAD II model with DLR reference data showed good agreement; see Ref. 8. The deflection of the active-camber section was prescribed. Inertial effects due to dynamic actuation as well as chordwise elastic deformation were not considered. Baseline rotor blade structural properties were assumed throughout the rotor blade span where not denoted differently; see Fig. 2.

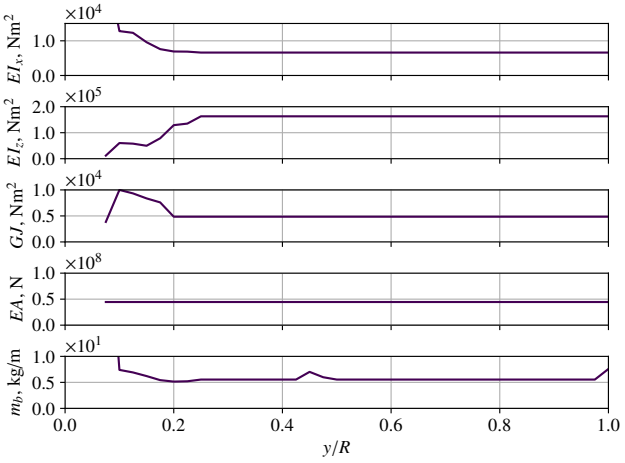

Fig. 2. Rotor blade structural properties; blade flap bending stiffness (EI_x), blade lag bending stiffness (EI_z), blade torsional stiffness (GJ), blade axial stiffness (EA), blade mass (m_b).

Aerodynamics Model

The calculation of aerodynamic forces in the comprehensive analysis was based on lifting-line theory, evaluating 2-D airfoil characteristics at discrete radial stations. These airfoil characteristics for the baseline NACA23012 and camber morphed profiles were computed with RANS CFD simulations (Ref. 10). In spanwise direction, the blade was discretized using 28 aerodynamic panels, distributed nonuniformly over the blade. All analyses were carried out using 24 azimuthal stations per revolution, i.e., an azimuthal time step size of $\Delta\psi = 15^\circ$. The rotor wake was calculated using a four-trailer free vortex wake analysis with two trailers enclosing the aerodynamically active part of the rotor blade, i.e., placed at the most inboard ($0.22R$) and outboard ($1.00R$) radial stations. Inboard of $0.22R$ the aerodynamics were not modeled. The remaining two trailers enclosed the active-camber blade section, where the morphing concept was implemented. Full wake distortion was computed and vortex roll-up was modeled without consolidation of trailers. The wake geometry was truncated after five rotor revolutions in fast forward flight, and 17 rotor revolutions in hovering flight until full convergence of the simulations was achieved. A single-peak model was used to determine the bound vorticity at the rotor blade.

The baseline Bo 105 rotor blade was not tapered and included a linear twist from hub to tip of $\theta_{tw} = -8^\circ$. This translated into a linear twist within the aerodynamically active blade section (from $0.22R$ to $1.00R$) of -6.24°.

Trim Condition and Validation

The trim conditions for the present active rotor study are detailed in Table 1. A propulsive trim was used in correspondence to a Bo 105 free-flight test campaign (Ref. 11). Hence, the rotor physics were supposed to be representative of a realistic flight condition. Since active rotor inputs affected the rotor aerodynamics, it was required to re-trim the rotor for investigations involving camber actuation to match the trim targets detailed in Table 1. A thrust of $T = 27520$ N corresponded to $C_T/\sigma = 0.886$.

Table 1. Trim conditions used for the active-camber study.

μ	$\alpha_s(^\circ)$	L (N)	M_x (Nm)	X (N)
0.00	0	27520	1400	0
0.05	-1	27520	1000	-72
0.10	-2	27520	600	-289
0.15	-3	27520	500	-652
0.20	-4	27520	600	-1149
0.25	-5	27520	700	-1802
0.30	-6	27520	1000	-2609
0.35	-7.3	27520	1400	-3572

The computational framework used in this study was validated for $\mu = 0.3$ based on a full-scale Bo 105 wind tunnel test (Ref. 12). Trim angles, rotor power, and structural loads showed good agreement between measurements and computations. The full validation of this comprehensive analysis model was presented in Ref. 8. Additionally, an advance ratio sweep was conducted to compare the rotor power with free flight test data (Ref. 9).

Results and Discussion

Based on the results obtained in a previous study (Ref. 8), best rotor performance improvement in fast forward flight ($\mu = 0.3$) was obtained using a 40% R span active-camber section that was centered at 70% R (Ref. 8). For consistency, unless explicitly stated, this configuration was also used in the current study for all advance ratios, notwithstanding that

some additional benefits were obtained at low-speed flight by extending the active-camber section towards further inboard radial stations (Ref. 9).

All of following forward flight results were based on spanwise uniform 0P+1P camber actuation (that is, mean deflection combined with 1/rev harmonic amplitude) which aimed to cover most of the potential to improve rotor power by blade active camber actuation (Ref. 8). The shown active rotor cases always refer to the most efficient camber deployment schedule in terms of rotor power savings for each single configuration and operating condition. These were determined by a parametric study with subsequent local search optimization. For hovering flight, always a quasi-static (0P) camber deflection was used, because a dynamic (1P or higher) camber actuation did not result in any significant benefits in terms of rotor power savings. Instead, spanwise variation of camber deflection yielded some additional power savings and was also investigated for a number of hovering flight cases.

In Fig. 3, the rotor power savings from active camber are shown for different blade loadings, C_T/σ. Here, the baseline rotor properties remained unmodified. Instead, C_T/σ was varied through a variation of rotor thrust. P_b refers to the power of the original baseline rotor and trim condition (see Table 1), which in this case was the rotor power based on the reference $C_T/\sigma \approx 0.0886$. $P_{\mathrm{b,mod}}$ refers to the modified rotor or operating condition (C_T/σ in this case), also without active-camber actuation.

As shown here, C_T/σ affected the rotor power improvement from active camber. With higher C_T/σ the relative power savings were improved. This is explained by the fact that increasing thrust was more efficient when cambering the blade airfoil rather than just increasing the angle of attack. Accordingly, active camber not only reduced the required rotor power for such cases, but presumably is also suited to increase the maximum take-off weight of a rotorcraft.

To isolate the specific effects from modifying the baseline rotor, all following investigations (except for RPM variation) were conducted maintaining the original rotor blade loading.

Blade Torsional Stiffness

Active-camber actuation results in complex aeroelastic interactions including elastic twisting of the rotor blade. To identify the influence of this induced elastic twist on the rotor power improvement from active camber, the torsional stiffness of the rotor blades, GJ, was varied and the result is shown in Fig. 4. The optimum rotor power obtained using active camber varied significantly in low-speed flight, but not in high-speed flight; see Fig. 4a. The relative improvement from active camber, in contrast, varied notably with GJ for low and high speeds; see Fig. 4b.

This different behavior was caused by the considerable difference in the efficiency in high-speed flight using the passive rotor with different GJ. Thus, active camber compensated any lack of efficiency originated in the torsional softness of the rotor blade in high-speed flight. This means that for high-speed flight no design target can be deduced for GJ with regard to optimum rotor power using active camber. Only the relative improvement increased with the torsional softness of the rotor blade. Although the relative improvement from active camber was significantly reduced in case of the quasi-rigid configuration, $GJ = 1000\%$, still some amount of relative improvement was produced. This was assumed to be originated in the improved airfoil aerodynamic efficiency from actively adjusting the blade camber.

From $\mu = 0$ to $\mu = 0.20$, torsional stiffness had considerable influence on best rotor efficiency using active camber. This was ascribed to the amount of required blade twist for optimum rotor power in low-speed flight. With high torsional blade stiffness, active camber was less effective in inducing elastic blade twist, which is one way in which active camber works to distribute aerodynamic loads more uniformly over the rotor disk. The amount of power improvement with a torsional soft configuration was further favored by the low built-in twist of the baseline rotor.

The induced elastic twist, θ_{etw}, of a high-speed flight case ($\mu = 0.3$) is shown in Fig. 4c. While θ_{etw} was negligible in case of $GJ = 1000\%$, it increased with torsional softness of the rotor blade yielding high elastic twisting of the rotor blade up to -8° with $GJ = 80\%$. Highest actuation amplitudes were required for cases with medium torsional stiffness ($GJ = 100\%$ and $GJ = 120\%$); see Fig. 4d.

Built-in Blade Twist

Improving rotor power with active camber in low-speed flight mainly resulted from a redistribution of thrust from outboard to further inboard radial stations. Such a redistribution can also be achieved by increasing the built-in twist of the rotor blade, θ_{tw}. However, greater twist overall may result in power penalties in high-speed flight. Nevertheless, while greater values of θ_{tw} improved rotor power in low-speed flight, no performance penalty was obtained at high-speed flight up to $\theta_{\mathrm{tw}} = -14^\circ$. This suggests that the built-in blade twist of the baseline Bo 105 rotor was below the optimum, as also stated in Ref. 13.

Since part of the reduced efficiency at low forward speeds due to the low built-in twist was compensated by the active-camber deflection, greater blade twist resulted in a relative reduction of power savings from active camber; see Figs. 5a and 5b. Therefore, with the Bo 105 rotor as the baseline rotor (which is a relatively low-twist rotor) benefits from the active camber mechanism were moderately overestimated in low-speed flight compared to those obtainable on a modern rotor with higher built-in twist.

At high forward speeds, relative power savings from active camber decreased up to $\theta_{\mathrm{tw}} = -14^\circ$; see Fig. 5b. When further increasing the built-in twist, benefits from active camber increased again, countering the power penalties due to high built-in blade twist. In terms of total rotor power (see Fig. 5a), the highest efficiency was obtained using active camber for built-in baseline twist values of $\theta_{\mathrm{tw}} = -6^\circ$ to $\theta_{\mathrm{tw}} = -10^\circ$.

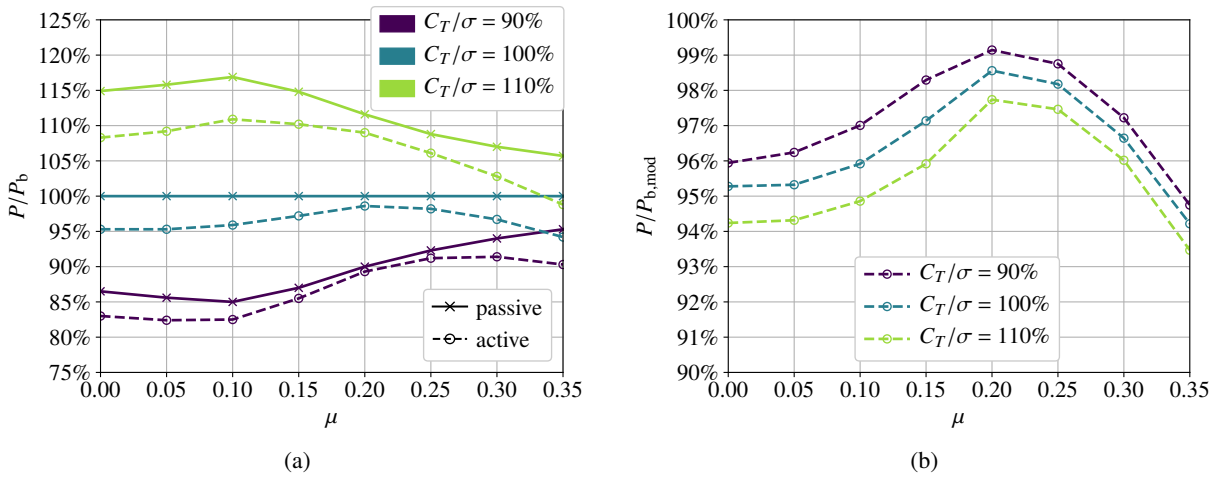

Fig. 3. Variation of the the rotor blade loading coefficient, C_T/σ, based on different thrust. (a) Rotor power relative to reference baseline case ($C_T/\sigma \approx 0.0886$), (b) Power savings from active camber related to the corresponding (adjusted C_T/σ) passive baseline cases.

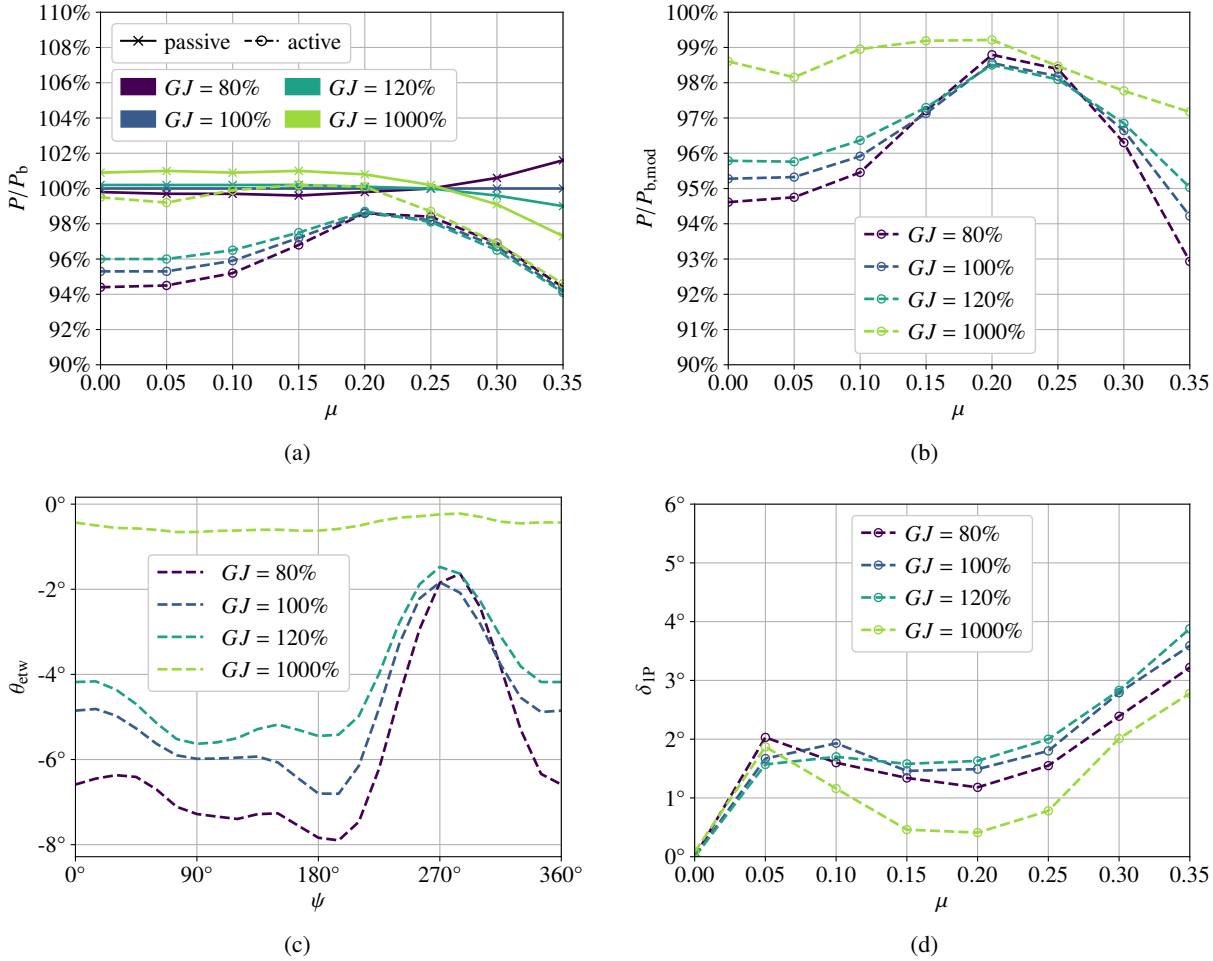

Fig. 4. Variation of blade torsional stiffness, GJ, for different advance ratios. (a) Rotor power relative to the original baseline rotor, (b) Power savings from active camber related to the corresponding (modified) passive baseline rotors, (c) blade elastic twist at $\mu = 0.3$ with active-camber actuation, (d) Active camber 1P amplitude.

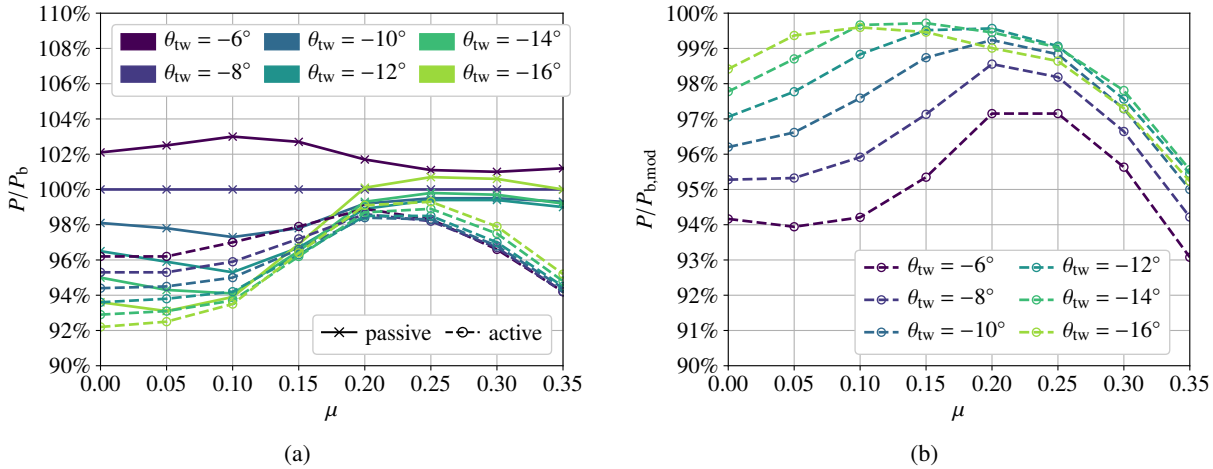

(a) (b)

Fig. 5. Variation of the built-in blade twist, θ_{tw}, for different advance ratios. (a) Rotor power relative to the original baseline rotor, (b) power savings from active camber related to the corresponding (modified θ_{tw}) passive baseline rotors.

A detailed analysis of hovering flight is provided in Fig. 6. It shows a comparison of different camber section sizes and a comparison of spanwise uniform and spanwise varying camber deflection. While lowest required power in fast forward flight was obtained for $\theta_{tw} = -6°$ to $\theta_{tw} = -10°$ when using active camber, the hovering case was most efficient for $\theta_{tw} = -14°$ to $\theta_{tw} = -16°$ and resulted in about 9% improvement over the passive baseline Bo 105 rotor; see Fig. 6a. Although these cases resulted in the lowest relative power savings from active camber (see Fig. 6b), still more than 4% rotor power savings were obtained with $\theta_{tw} = -14°$ in hovering flight when using spanwise varying camber deflection ($\vartheta = 40\%$ to $\vartheta = 80\%$) and an active-camber section from $r_1 = 0.22R$ to $r_2 = 0.90R$. This was about double the amount of the improvement that was possible with the smaller section (applied between $r_1 = 0.50R$ and $r_2 = 0.90R$) and spanwise uniform deflection.

Consequently, a built-in twist value of about $\theta_{tw} = -12°$ was an appropriate compromise when using active camber. Without active-camber actuation, a built-in twist of $\theta_{tw} = -14°$ was most efficient in terms of rotor power.

With respect to the camber actuation deployment, mainly the mean camber deflection was affected from changing the built-in twist; see Fig. 7. With higher values of θ_{tw}, the requirement for mean camber deflection was significantly reduced. For high-speed flight, this resulted in negative camber deflections on the advancing side. For low built-in twist, positive camber deflections were required over the entire azimuth range.

Blade Taper Ratio

Linear taper was applied to the untapered ($t = c_{tip}/c_{root} = 100\%$) (i.e., original) Bo 105 rotor blade, while maintaining the original rotor solidity of $\sigma = 0.07$. A clear trend was obtained that the rotor power from the passive rotor was improved by introducing blade taper; see Fig. 8a. However, in contrast to the built-in twist, this improvement in baseline rotor efficiency did not adversely affect the relative improvement obtained from active-camber actuation; see Fig. 8b. In hovering and high-speed flight, the relative power savings obtained from active camber even increased when tapering the rotor blades. Introducing rotor blade taper was particularly efficient for advance ratios where active camber alone was less successful. Hence, blade taper and active blade camber appeared to provide good synergy and acted in a complementary fashion.

Rotor Rotational Speed

The effect of varying the rotor rotational speed, or rotations per minute, RPM, on rotor power is shown for active and passive cases in Fig. 9. Since forward flight velocity varies with rotor RPM for constant μ, this comparison was done based on the same forward flight velocities. Rotor geometry, structural properties, and trim forces remained unmodified, which resulted in different C_T/σ for different rotational speeds.

Figure 9a shows that lower RPM resulted in a reduction of rotor power over the entire investigated flight envelope. Higher-than-baseline RPM resulted in a distinct rotor power penalty. This was ascribed to the increase in drag from higher Mach numbers, especially close to the blade tip. The relative power reduction from active camber was moderately reduced with lower RPM (see Fig. 9b). However, in absolute terms, the combination of RPM reduction and active camber was clearly more efficient than any higher RPM case; see Fig. 9a.

Possible disadvantages from such slowed rotor configurations are a reduction in maximum rotor thrust/lift and dynamic stall (or reduced stall margin) in fast forward flight. These detriments, however, were largely countered by using active-camber actuation; see Fig. 10. As shown in Fig. 10a, the angle of attack, α, decreased with higher rotational speed, ultimately resulting in a greater $C_{l,max}$ margin over the entire rotor blade. A similar effect resulted from using active camber; see Fig. 10b. In high-speed flight and without active camber, higher rotational speeds resulted in lower maximum α from low to medium Mach numbers; see Fig. 10c. At high Mach numbers, slightly higher α were observed with higher rotational speed. Comparing the active and passive case based on

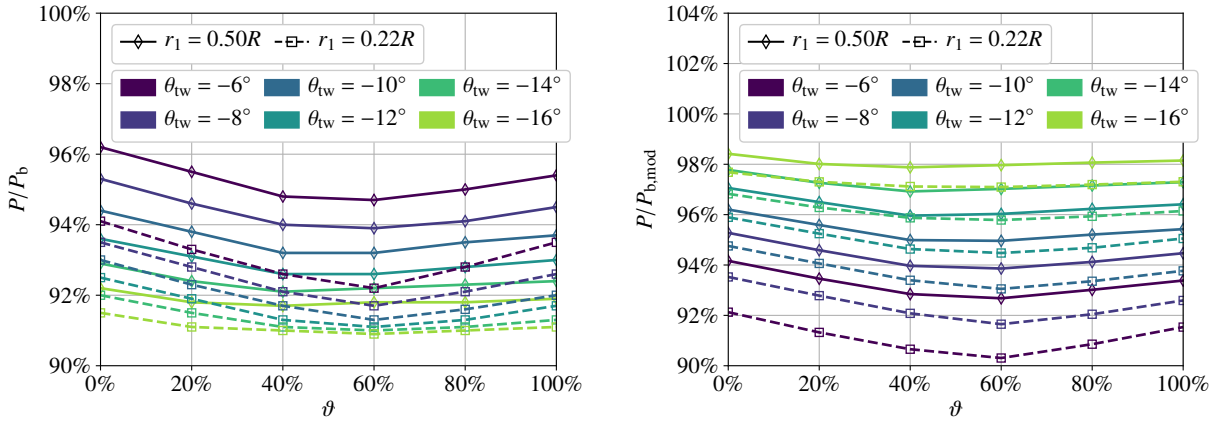

Fig. 6. Power savings in hovering flight from spanwise varying camber deflection for different built-in blade twist, θ_{tw}, and different active-camber section sizes (active-camber section implemented between r_1 and $r_2 = 0.90R$). (a) Rotor power relative to the original baseline rotor, (b) power savings from active camber related to the corresponding (modified θ_{tw}) passive baseline rotors.

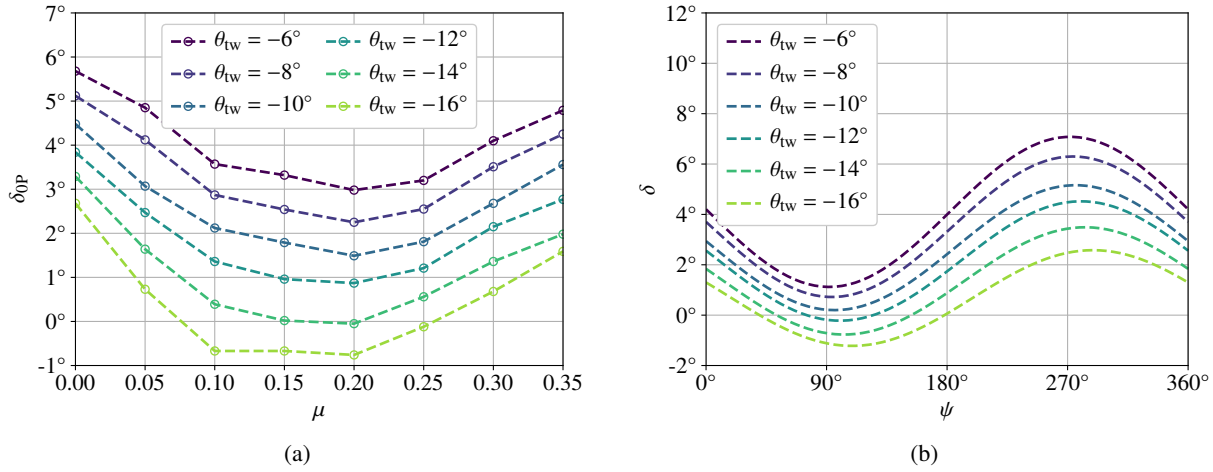

Fig. 7. Variation of the built-in blade twist, θ_{tw}. (a) Active camber (0P) mean camber deflection, (b) Active-camber actuation profile over the rotor azimuth for $\mu = 0.3$.

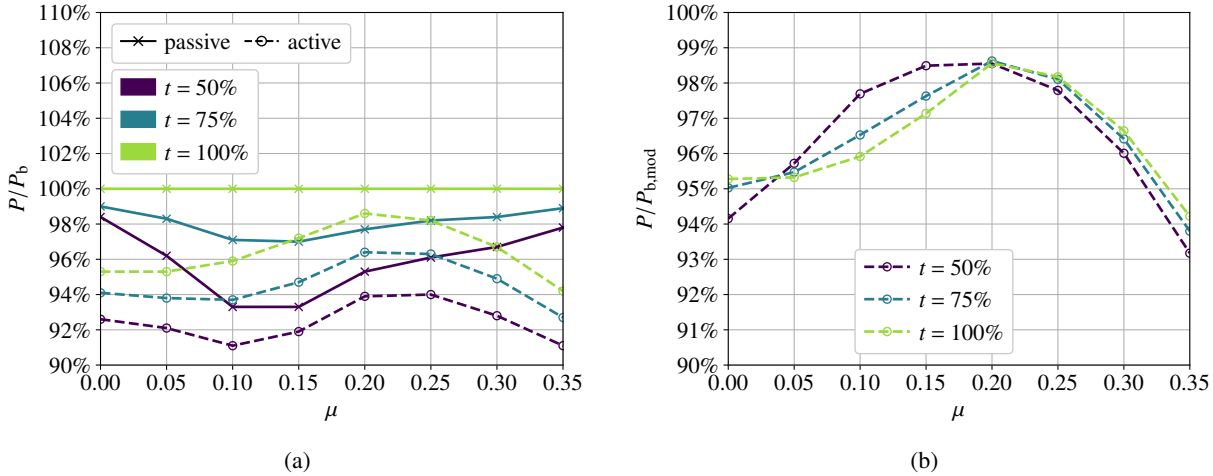

Fig. 8. Variation of the taper ratio, $t = c_{tip}/c_{root}$, for different advance ratios. (a) Rotor power relative to the original baseline rotor ($t = 100\%$), (b) power savings from active camber related to the corresponding (modified t) passive baseline rotors.

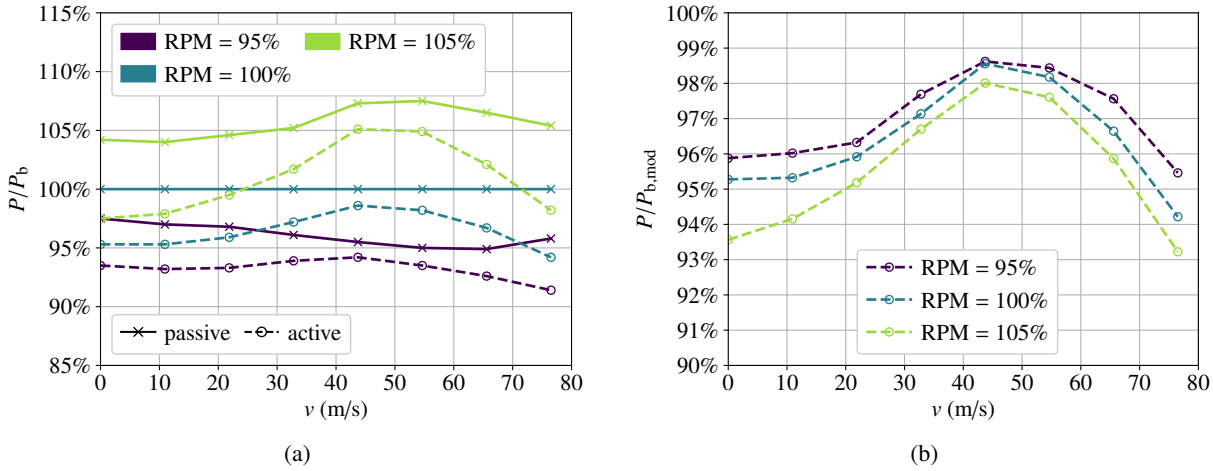

(a) (b)

Fig. 9. Variation of the rotor rotational speed (in RPM) for different forward flight velocities. (a) Rotor power relative to the original baseline rotor, (b) power savings from active camber related to the corresponding (modified RPM) passive baseline rotor.

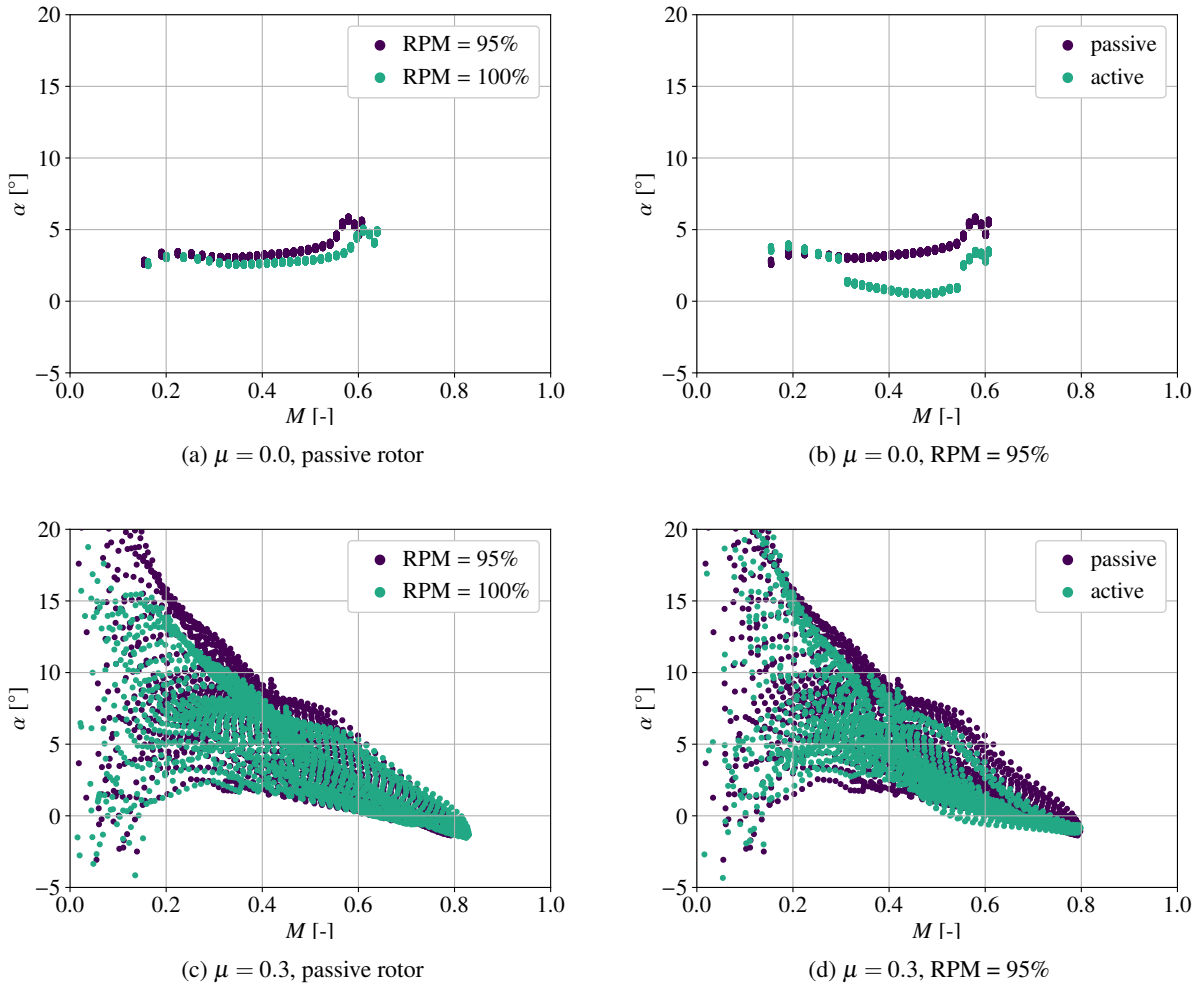

(a) $\mu = 0.0$, passive rotor

(b) $\mu = 0.0$, RPM = 95%

(c) $\mu = 0.3$, passive rotor

(d) $\mu = 0.3$, RPM = 95%

Fig. 10. Blade sectional angles of attack, α, and corresponding Mach numbers, M, appearing on the rotor disk. (a) and (c) Comparison of passive cases with different rotor rotational speed (in RPM), (b) and (d) comparison of passive and active camber cases based on RPM = 95%.

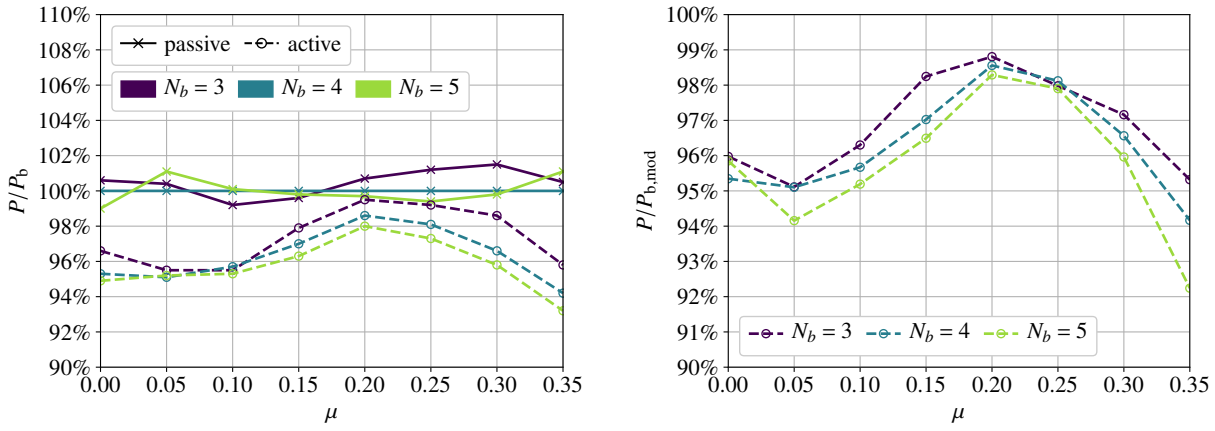

Fig. 11. Variation of the number of rotor blades, N_b, for different forward flight velocities. (a) Rotor power relative to the original baseline rotor, (b) power savings from active camber related to the corresponding (modified N_b) passive baseline rotors.

RPM= 95%, lower maximum α were required from medium to high Mach numbers; see Fig. 10d.

For the investigated conditions and rotors, the active camber mechanism allowed a reduction in RPM of about 5% while compensating for the disadvantages associated with this rotational speed reduction. This means that in addition to the primary effect of directly reducing rotor power, active camber may further improve rotor power as a secondary effect by allowing RPM reduction of up to 5%. The aforementioned compensation appeared when explicitly optimizing for minimum rotor power for a given RPM. Therefore, blade sectional angles of attack and stall margins may presumably further be reduced by considering them as additional optimization targets. Overall, power savings over the original baseline rotor at low speed were up to 6-7% for at low forward speeds, 5-6% at medium speed, and 8-9% in high-speed flight, which is expected to increase further when applying spanwise varying active-camber actuation on a larger active-camber section in low-speed flight, and a superposition of 1P+2P actuation in high-speed flight (Ref. 9).

Number of Rotor Blades

For the comparison of different numbers of rotor blades, N_b, blade chord, c, was adjusted to maintain the original C_T/σ. As a consequence, structural properties were adjusted to ensure a dynamically similar behaviour and constant rotor mass. Varying N_b only moderately affected the rotor power and no clear trend was observed regarding the efficiency of the passive rotor; see Fig. 11b. The relative power improvement from active camber was moderately affected by the number of rotor blades; see Fig. 11b. Here, the trend was observed that slightly greater power savings were obtained with a higher number of rotor blades. Hence, in terms of the total rotor power for combinations of different N_b and active-camber actuation, the five-bladed rotor yielded the highest efficiency. It resulted in 0.5% to 1% of additional power improvement compared to the four-bladed Bo 105 rotor from $\mu = 0.15$ to $\mu = 0.35$.

Conclusions

The effects of varying a number of Bo 105 main rotor properties and operating conditions on rotor power savings from active camber were computationally investigated over a range of advance ratios from hover to 0.35. All investigations used 0P+1P harmonic actuation, which previously was found to cover the major part of power saving capability from active camber. The following conclusions have been drawn:

- A reduction in torsional stiffness resulted in more relative power improvement from active camber. However, only at low and medium speed this also resulted in lower absolute rotor power. In high-speed flight, the active-camber mechanism was capable of compensating any power penalty emerging from blade torsional softness. In low-speed flight, high power reductions were attributed to the low built-in blade twist.

- With higher built-in blade twist, the capability to improve rotor power by using active camber decreased significantly at low speeds, and moderately at high speeds (at high speed only up to $\theta_{tw} = -14°$). Still, more than 4% rotor power savings were obtained in hovering flight with $\theta_{tw} = -14°$ when using an extended active-camber section ($r_1 = 0.22R$ to $r_2 = 0.90R$) and spanwise varying deflection. In high-speed flight, best overall rotor power was obtained from a combination of low to moderate twist ($\theta_{tw} = -6°$ to $\theta_{tw} = -10°$) and active-camber actuation.

- Baseline power consumption was significantly improved when applying a taper ratio of $t = 50\%$. Additionally, for a large range of advance ratios, the relative improvement from active camber was slightly higher when used in combination with blade taper as compared to rectangular blades using active camber. This indicated that improved efficiency of the baseline rotor does not necessarily result in less power savings from active camber.

- Active camber was slightly more effective on a five-bladed rotor than on a four- or three-bladed rotor, yielding more than 7% power savings in high-speed flight compared to 6% on a four-bladed rotor. Also, rotor total power required was lowest in case of the five-bladed rotor using active-camber actuation.
- When reducing rotor rotational speed by 5%, baseline rotor power improved significantly over the entire flight envelope investigated. Simultaneously, power savings from active camber were slightly decreased. However, the lack of lift production capability due to low rotational speed was efficiently compensated by active camber. Thus, active camber may facilitate a reduction in rotor rotational speed and thereby increase overall rotor efficiency further. In combination, more than 6% power savings were obtained in low-speed flight, more than 5% in medium-speed flight, and more than 8% in high-speed flight conditions.

Overall, the promising technology of active blade camber variation efficiently reduced rotor power when applied to a wide range of baseline rotor designs that are representative of modern rotor designs. The active-camber results from the original Bo 105 main rotor were benefited by the low built-in twist of this rotor, especially in low-speed flight. However, even greater power savings were found when the active camber mechanism was used in combination with other efficiency oriented rotor design choices such as blade taper. High potential was shown for an actively cambered blade as applied to a slowed rotor concept, further reducing rotor power requirements and simultaneously countering the disadvantages emerging from the rotational speed reduction, such as the reduced lift capability and issues with the stall margin.

Author contact:

Dominik Komp: dominik.komp@tum.de
Manfred Hajek: hajek@tum.de
Jürgen Rauleder: juergen.rauleder@gatech.edu

Acknowledgments

This project has received funding from the European Union's Horizon 2020 research and innovation program under grant agreement No. 723491.

References

[1]Nguyen, K. Q. and Chopra, I., "Application of Higher Harmonic Control to Hingeless Rotor Systems," Technical Report 103846, NASA TM, March 1991.

[2]Jacklin, S. A., Blass, A., Swanson, S. M., and Teves, D., "Second Test of a Helicopter Individual Blade Control System in the NASA Ames 40- by 80-Foot Wind Tunnel"," American Helicopter Society 2nd International Aeromechanics Specialists Conference, Bridgeport, CT, October 1995.

[3]Jain, R., Yeo, H., and Chopra, I., "Computational Fluid Dynamics - Computational Structural Dynamics Analysis of Active Control of Helicopter Rotor for Performance Improvement," *Journal of the American Helicopter Society*, Vol. 55, (4), 2010.
doi: 10.4050/JAHS.55.042004

[4]Jain, R., Yeo, H., and Chopra, I., "Examination of Rotor Loads Due to On-Blade Active Controls for Performance Enhancement," *Journal of Aircraft*, Vol. 47, (6), 2010.
doi: 10.2514/1.C000306

[5]Ravichandran, K., Chopra, I., Wake, B. E., and Hein, B., "Trailing-Edge Flaps for Rotor Performance Enhancement and Vibration Reduction," *Journal of the American Helicopter Society*, Vol. 58, (2), April 2013.
doi: 10.4050/JAHS.58.022006

[6]Liu, L., Friedmann, P. P., Kim, I., and Bernstein, D. S., "Rotor Performance Enhancement and Vibration Reduction in Presence of Dynamic Stall Using Actively Controlled Flaps," *Journal of the American Helicopter Society*, Vol. 53, (4), 2008, pp. 338–350.
doi: 10.4050/JAHS.53.338

[7]Woods, B. K., Bilgen, O., and Friswell, M. I., "Wind Tunnel Testing of the Fish Bone Active Camber Morphing Concept," *Journal of Intelligent Material Systems and Structures*, Vol. 25, (7), 2014, pp. 772–785.
doi: 10.1177/1045389X14521700

[8]Komp, D., Kumar, S., Hajek, M., and Rauleder, J., "Effect of Active Camber Morphing on Rotor Performance and Control Loads," *Aerospace Science and Technology*, 2020, pp. 106311.
doi: 10.1016/j.ast.2020.106311

[9]Komp, D., Hajek, M., and Rauleder, J., "Rotor Performance Enhancements with Spanwise Varying Active Camber Morphing," AIAA Scitech 2021 Forum.
doi: 10.2514/6.2021-0200

[10]Abdelmoula, A. and Rauleder, J., "Aerodynamic Performance of Morphed Camber Rotor Airfoils," AIAA Scitech 2019 Forum, January 2019.
doi: 10.2514/6.2019-1101

[11]Langer, H. J. and Tränapp, N., "BO 105 Flight Test Data for a Wind Tunnel Test Program," Dlr ib 111–93/58, 1993.

[12]Peterson, R. L., Maier, T. H., Langer, H. J., and Tränapp, N., "Correlation of Wind Tunnel and Flight Test Results of a Full-Scale Hingeless Rotor," American Helicopter Society Aeromechanics Specialist Conference, San Francisco, CA, January 1994.

[13]Braun, D. and Humpert, A., "BO105 CBS-5: BO105 upgrade through new rotor blades," *19th European Rotorcraft Forum, Italy*, 1993.